Study of the Noise Mechanisms of Transonic Blade-Vortex Interactions

A. S. Lyrintzis* and Y. Xue†
University of Minnesota, Minneapolis, Minnesota 55455

Transonic blade-vortex interactions (BVI) are simulated numerically and the noise mechanisms are investigated. The two-dimensional high-frequency transonic small-disturbance equation is solved numerically (VTRAN2 code). An alternating direction implicit (ADI) scheme with monotone switches is used; viscous effects are included on the boundary and the vortex is simulated by the cloud-in-cell method. The Kirchhoff method is used for the extension of the numerical two-dimensional near-field aerodynamic results to the linear acoustic three-dimensional far field. The viscous effect (shock/boundary-layer interaction) on BVI is investigated. The different types of shock motion are identified and compared. Two important disturbances with different directivity exist in the pressure signal and are believed to be related to the fluctuating lift and drag forces. Noise directivity for different cases is shown. The maximum radiation occurs at an angle between 60 and 90 deg below the horizontal for an airfoil-fixed coordinate system and depends on the details of the airfoil shape. Different airfoil shapes are studied and classified according to the BVI noise produced.

Introduction

AMONG the several types of helicopter noise,[1] that due to blade-vortex interactions (BVI) is one of the most important. BVI is the aerodynamic interaction of a rotor blade with the trailing vortex system generated by preceding blades as shown in Fig. 1 (from Ref. 2). It usually occurs during helicopter descent or low-speed maneuvers. It is loud, impulsive in character, and tends to dominate the other sources when it occurs, as shown experimentally (e.g., Schmitz and Yu[3]). Also, very complicated BVI patterns arise from tilt-rotor aircraft.[4] Interactions generate the most significant noise when they are intrinsically unsteady, as when the vortex is exactly parallel to the blade, or when the vortex is nearly parallel to the blade (a vertical interaction is steady for two-dimensional blade). Incompressible BVIs have been successfully treated in the past (e.g ., Ref. 5). For typical helicopter cases though, it was shown in Ref. 6 and 7 that the aerodynamics and aeroacoustics of the interactions are intrinsically transonic. In such cases, the flow can be initially modeled by two-dimensional unsteady transonic flow (Fig. 2).

Unsteady transonic flow problems have been solved numerically in the past. The low-frequency approximation of the unsteady two-dimensional transonic small-disturbance (TSD) equation was first solved by Ballhaus and Goorjian,[8] and the LTRAN2 code was created. Since then, the code has been updated to include high-frequency effects,[9] viscosity,[10] monotone switches,[11] and second-order effects.[12] However, the acoustic waves resulting from the unsteady motion have not been adequately studied.

Two-dimensional transonic BVI was first studied computationally in the near- and midfield by George and Chang[6,7] who used the high-frequency transonic small-disturbance equation, including regions of convected vorticity. References 6 and 7 also contain detailed discussions of the background and formulation of the transonic BVI problem. A comprehensive code, VTRAN2 was developed[13,14] as a modification of LTRAN2 to include the vortex. The vorticity is bilinearly distributed inside a vortex core and branch cuts are introduced in the x direction. The vortex can either follow a prescribed path, or can be convected with the freestream. A new look at the physics of the acoustics of unsteady transonic flow was given in Ref. 15. In Refs. 16–24, the two-dimensional transonic BVI problem is also solved using the small-disturbance theory and the more complex Euler and thin-layer Navier-Stokes equations. Also Baeder et al.[22,23] and Liu et al.[24] presented some near- and midfield results. At great distances from the airfoil though, the waves become very difficult to follow because of numerical diffusion and dispersion errors.

Kirchhoff's method was introduced[14,25–29] to extend the numerically calculated nonlinear aerodynamic results to the linear acoustic far field. This method uses a Green's function for the linearized governing equation to derive a represen-

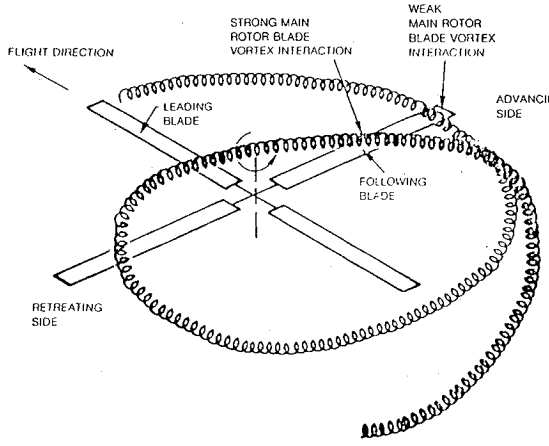

Fig. 1 Formulation of BVI for a four-bladed rotor (from Schlinker and Amiet[2]).

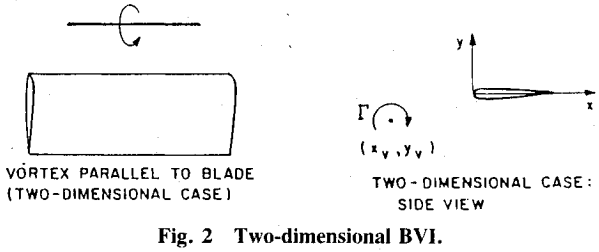

Fig. 2 Two-dimensional BVI.

Received Sept. 12, 1990; revision received Jan. 28, 1991; accepted for publication Feb. 20, 1991.

*Assistant Professor, Aerospace Engineering and Mechanics. Member AIAA.

†Graduate Student, Aerospace Engineering and Mechanics. Member AIAA.

tation for the solution in terms of its values and derivatives on a closed surface S in space, which is assumed to include all of the nonlinear flow effects and noise sources. The potential and its derivatives can be numerically calculated from a nonlinear aerodynamic code (e.g., VTRAN2). The Kirchhoff method has the advantage of including the full diffraction effects and eliminates the erroneous propagation of the reactive near field.

In this paper, we examine the noise due to BVI. An existing code (VTRAN2) was enhanced to include monotone switches and viscous effects. The viscous effects (shock/boundary-layer interaction) on BVI noise are studied. The resulting noise because of the different types of shock-wave motion types in the near and the far field is investigated and the different resulting disturbances are analyzed. The noise mechanisms are explained physically and the relation between the noise signal and oscillating lift and drag forces is shown. The complicated directivity patterns of BVI noise are also studied. Different airfoil shapes are studied and classified according to the produced BVI noise.

Numerical Method (VTRAN2)

VTRAN2 is a code[13,14] developed for analyzing the interactions of convected regions of vorticity with airfoils using transonic small-disturbance theory. It is based on the ADI implicit scheme of the LTRAN2 code[8] with the inclusion of the high-frequency term as described in Ref. 9 and the addition of regions of convected vorticity using the cloud-in-cell and multiple branch-cut approach. The code was modified to include viscosity[8] and monotone switches.[10]

The governing equation for the unsteady transonic small-disturbance potential and the boundary conditions can be found in various references (e.g., Refs. 25 and 30). The classical Kutta condition is satisfied by this small-disturbance formulation. We are interested in cases for which the reduced frequency range is less than 4, which is the limit for the application of the Kutta condition.[31] A finite vortex core is used (cloud-in-cell method) for reasons of computational stability. The core has a finite square shape limited by grid lines and the vorticity is bilinearly distributed inside. Thus, several branch cuts (in the x direction) are introduced. The vortex can have a free path (convected by the flow) or a prescribed path (miss distance y_v = const, vortex velocity = U_o). Details of the theoretical formulation were given by Chang[32] and Lyrintzis.[14]

For the viscosity calculations the viscous-ramp method (wedge) is used. The viscous-ramp model simulates the shock/boundary-layer interaction by placing a wedge-nosed ramp at the base of the shock to obtain the reduced shock pressure rise. The surface geometry must be augmented by the ramp model by adding an extra viscous term in the boundary condition. Details of the calculation of that viscous term can be found in Ref. 33. The ramp model was derived for steady-state computations. However, it can be incorporated into unsteady computations in a quasisteady fashion. Thus, the model is valid for low frequencies, and its use in high-frequency problems such as BVI can only give some qualitative information about the effect of viscosity with almost no additional CPU time. The more complicated and CPU time-consuming lag-entrainment method which was also incorporated in our code was not used, because it was not superior to the wedge model for unsteady cases.[33]

An ADI method is used for the solution of the equation, where the high-frequency term is added in the y sweep. An approximate factorization technique with monotone switches[11] is used for the steady calculation, which provides a startup solution. Special care is taken for the conservative differentiation along the uneven mesh.

A 213×199 mesh is used for the calculations. The computational mesh points are clustered more densely near and in front of the airfoil and are stretched exponentially from the near airfoil region to about 200 chords from the airfoil in the x direction and 400 chords in the y direction. More mesh points are added in the y direction for the more accurate evaluation of the normal derivatives on the Kirchhoff surface. The VTRAN2 code was shown to agree well with other, more complex approaches including Euler and thin-layer Navier-Stokes computations.[7] The code has a high vectorization level and the CPU time for each two-dimensional case on a Cray-2 computer is about 4 min for 800 time-marching steps.

Kirchhoff's Method for the Far Field

In the past acoustic analogy has been used for the evaluation of noise signals. This approach starts from the calculation of the nonlinear near field and midfield and the far field is found from surface and volume integrals of near- and midfield flow and body surfaces. We should note that there are substantial difficulties in including the nonlinear quadrupole term (which requires second derivatives) in the volume integrals, especially around shock surfaces. Thus, a lot of investigators use near field data only on the blade surface, which is less accurate as shock surfaces are not included in the calculation.

Kirchhoff's method includes the calculation of the nonlinear near field and midfield with the far field solutions found from a linear Kirchhoff formulation evaluated on a surface surrounding the nonlinear field. This method provides an adequate matching between the aerodynamic nonlinear near field and the acoustic linear far field. The full nonlinear equations are solved in the first region (near field), usually numerically, and a surface integral of the solution over the control surface gives enough information for the analytical calculation in the second region (far field). The advantage of the method is that nonlinear effects (e. g., shock waves) are accounted for. Also, the surface integrals and the first derivatives needed can be easily evaluated from the near-field CFD data; full diffraction and focusing effects are included while eliminating the propagation of the reactive near field.

The Kirchhoff equation for a moving surface was originally derived by Morgans.[34] A Green's function approach will be used to rederive the Kirchhoff formula in a coordinate system fixed to the airfoil which moves with velocity U_o. The Green's function approach was introduced by Morino.[35,36] Farassat and Myers[37] rederived the Kirchhoff equation for an arbitrarily moving piecewise smooth deformable surface using generalized derivatives. A very brief discussion of the Kirchhoff formulation is given in the following paragraphs; for more details the reader is referred to the above references, and also Refs. 14 and 26.

A Green's function for the linearized governing equation is used to derive a representation for the solution in terms of its values and derivatives on a closed surface S in space, which is assumed to include all of the nonlinear flow effects and noise sources. A full three-dimensional formulation is used, because the Green's function is simpler in this case, and because the method can be easily extended to include spanwise variations to model three-dimensional BVI. The pressure distribution at a point (x_o,y_o,z_o) outside a rigid fixed surface is

$$p(x_o,y_o,z_o,t) = -\frac{1}{4\pi}\int_S \left[\frac{1}{r_o}\frac{\partial p}{\partial n_o} + \frac{1}{c_o r_o \beta^2}\frac{\partial p}{\partial t}\left(\frac{\partial r_o}{\partial n_o} - M\frac{\partial x'_o}{\partial n_o}\right) + \frac{p}{r_o^2}\frac{\partial r_o}{\partial n_o}\right]_\tau dS'_o \quad (1)$$

where

$$r_o = \{(x-x')^2 + \beta^2[(y-y')^2 + (z-z')^2]\}^{1/2} \quad (2a)$$

$$\tau = \frac{[r_o - M(x-x')]}{c_o\beta^2} \quad (2b)$$

$$\beta = (1-M^2)^{1/2} \quad (2c)$$

where the prime denotes a point on the Kirchhoff surface, subscript o denotes the transformed values using the well-known Prandtl-Glauert transformation:

$$x_o = x, \qquad y_o = \beta y, \qquad z_o = \beta z \tag{3}$$

n is the outward vector normal to the surface S, and subscript τ implies the evaluation at the retarded time $t_1 = t - \tau$.

Thus, the values of the potential and its normal derivatives on an arbitrary surface around the spanwise extent of an arbitrary flow are enough to give the far-field radiation at any arbitrary external point. In our work, we use as a control volume a rectangular box (Fig. 3) coinciding with mesh points in order to simplify the computation. The potential and its derivatives can be numerically calculated from an aerodynamic near-field code; then Eq. (1) is used to evaluate the solution in the far field. Thus, the solution is integrated on a surface in the midfield and nonlinear effects (e.g., shock waves) in the near field are fully accounted for.

Since Kirchhoff's method assumes that linear equations hold outside this control surface S, the latter must be chosen large enough to include the region of nonlinear behavior. However, due to increasing mesh spacing the accuracy of the numerical solution is limited to the region immediately surrounding the moving blade. Thus, S cannot be too large, because the numerical evaluation of the derivatives needed [Eq. (1)] is not accurate at large distances. Therefore, a judicious choice of S is required for the effectiveness of the Kirchhoff method. A rectangular box-shaped surface (Fig. 3) is used for the calculations. The VTRAN2 code is used to calculate the solutions on the surface S. The y limits of S for our calculations are varied over a range from $y_s = 0.25$ to 4.00 chords distance from the airfoil. Higher Mach numbers yield higher optimum values for y_s because of stronger nonlinearities in the larger lateral extent of the flow region. The x limits for S were also varied between 0.15 and 0.50 chords and, similarly, values of 0.25 chords upstream and downstream of the leading and trailing edges, respectively, are chosen.

Strip-theory approximation is used; that is, the two-dimensional VTRAN2 solution is applied on different segments of the blade in a stripwise manner. Blade segments ranging from 2 to 16 in aspect ratio are used. Usually mesh limitations keep the Kirchhoff surface close enough to the blade, where the two-dimensional strip-theory solution is still valid. By making calculations with or without the inclusion of the tip surfaces, we found[27] that they have only a small effect; thus they were neglected for most of the calculations.

Types of Unsteady Shock Motion

Tijdeman[38] showed experimentally, using an oscillating flap, that varying airfoil surface boundary conditions can give three different types of unsteady shock motion:

Type A shock motion, where the shock at the rear of the supersonic region merely moves back and forth with concurrent changes in strength.

Type B shock motion, where the shock moves similarly to type A, but disappears temporarily during the unsteady motion.

Type C shock motion, where the supersonic region disappears, but a shock wave leaves the airfoil and propagates forward to the far field.

The above three types of unsteady shock motions affect heavily the characteristics (e.g., lift, drag) of all unsteady transonic flows. The type of shock that occurs in a given situation depends on the flow characteristics (e.g., freestream Mach number, airfoil shape, amplitude, and frequency of the unsteady motion). These types of shock motion can even be observed in steady airfoils with severe flow separation downstream of the shock waves. Their existence in BVI has been verified by different experiments and calculations (e.g., Tangler's experiments[39]).

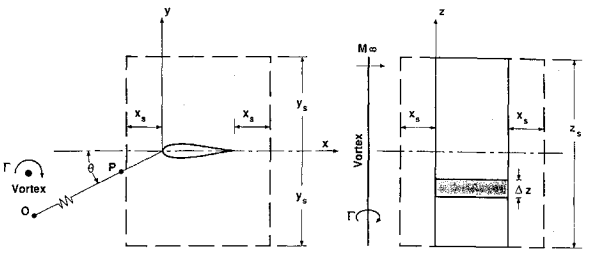

Fig. 3 Kirchhoff's surface for the calculation of the far field.

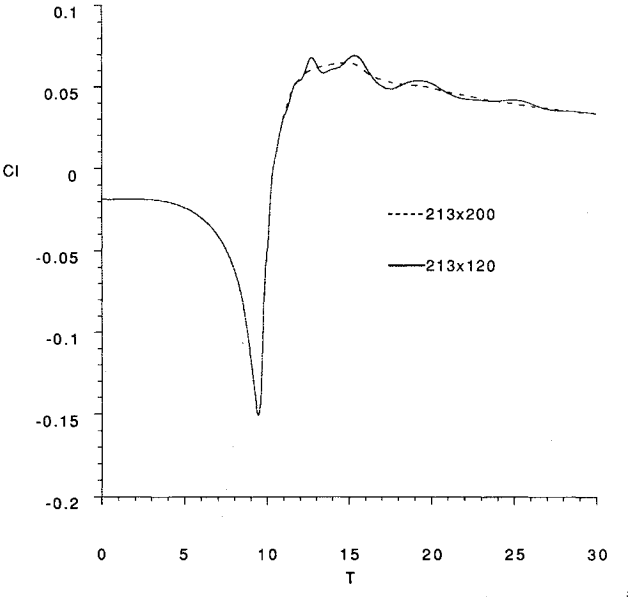

Fig. 4 Effect of y-grid size on the $C_l(T)$ signal for type C.

Results and Discussion

Some midfield calculations for BVI are performed using VTRAN2 with a refined mesh to follow the waves of interest. Then the Kirchhoff method is used to examine the noise at the far field. The calculations are made in an airfoil-fixed reference frame. A more detailed discussion of the coordinate systems used for BVI calculations is given in Ref. 25.

We use a NACA-64A006 airfoil; the vortex strength was $C_{lv} = 0.4$ (C_{lv} is a nondimensional measure of the vortex strength: $C_{lv} = 2\Gamma/cU_o$) and the vortex miss distance $y_o = -0.5$ chords, for a fixed vortex path. The initial vortex position is $x_o = -9.51$ chords and the freestream velocity is one (arbitrary units) so the vortex passes below the airfoil leading edge at time $T = 9.51$. The Mach numbers of 0.875, 0.854, and 0.822 correspond to shock wave motions of types A, B, and C, respectively, as also shown in Ref. 7. The three different types of the unsteady shock motion are thus studied. For the Kirchhoff surface (Fig. 3), we used a span of 8 chords, $x_s = 0.25$ chords and $y_s = 3.5$, 2.5, and 1.9 chords for the three types A, B, and C, respectively. Note that a larger y_s is required for higher Mach numbers, because the y extent of the nonlinear region of the flow increases, as expected from the scaling laws of transonic flow.

Figure 4 shows the effect of the grid on the lift coefficient $C_l(T)$. A standard 213×119 mesh is compared to a 213×199 mesh (finer in the y direction). The results show that the fine mesh produces a smoother solution. Smoother solutions are also produced for the pressure coefficient at different points, especially in the far field using the Kirchhoff method. Finer meshes were also tried, but the results were not substantially changed. Thus, the fine mesh (213×199) will be used in the subsequent calculations.

Figures 5–7 show the effect of viscosity in the calculations. The pressure coefficient $C_p(T)$ at point P (-0.3000, -0.17478), the lift coefficient $C_l(T)$, and the drag coefficient $C_d(T)$ are

plotted for a type A shock motion, for viscous and nonviscous calculations. We can see only a slight influence of the effect of viscosity. Since viscosity is added as an extra boundary condition to model shock/boundary-layer interaction, we expect the influence to be stronger with the increase of the strength of the shock. Thus, the effect of viscosity is lower for the types B and C (not shown) and zero for subcritical cases. The following results include the effect of the viscosity.

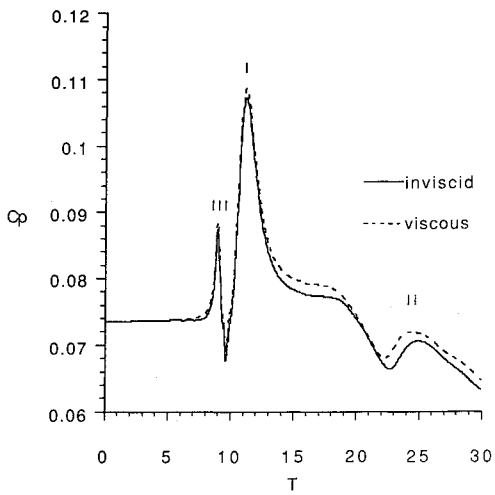

Fig. 5 Effect of viscosity on the $C_p(T)$ signal for type A [point P ($x = -0.3000$, $y = -0.17478$)].

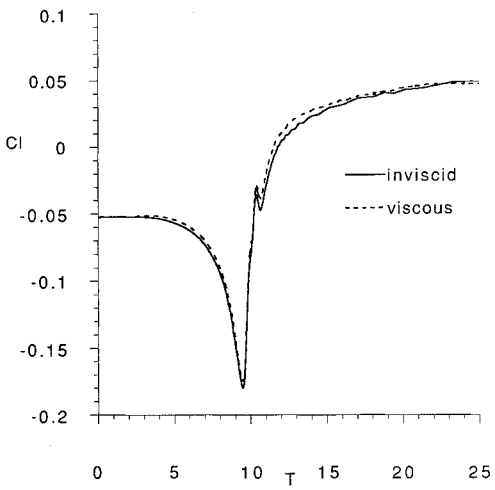

Fig. 6 Effect of viscosity on the $C_l(T)$ signal for type A.

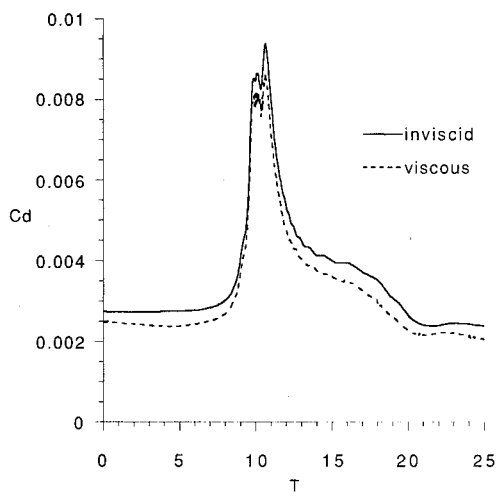

Fig. 7 Effect of viscosity on the $C_d(T)$ signal for type A.

Figures 8 and 9 show the $C_p(T)$ signal of the three types of unsteady shock motion in the midfield (point P) from VTRAN2 and in the far field (point O, $r = 20$ chords, $\theta = 30$ deg), as shown in Fig. 3, using Kirchhoff's method. The signal for the higher Mach number (type A) propagates upstream slower, so it takes a longer time to arrive at the same point (Fig. 9). The signal consists of three disturbances (I, II, III) as also shown in Refs. 25 and 26. The primary disturbance I is the main BVI noise and it originates at the airfoil when the vortex passes below the leading edge. It is believed to be related to the fluctuating lift coefficient C_l. The secondary disturbance II corresponds to the unsteady shock motion and depends on the motion of the entire supersonic region induced by the vortex passage. It originates at the airfoil at a later time, and depends heavily on the type of shock motion. It is believed to be somehow related to the fluctuating drag coefficient C_d. The time delay of disturbance II decreases with decreasing Mach number and disappears in subcritical cases. The directivity of the two disturbances is very different as will be shown later. The existence of the second disturbance was observed computationally by George and Chang[7] and was also verified experimentally by Caradonna et al.[40] and Shenoy,[41] and computationally by George and Lyrintzis,[25,26] Owen and Shenoy,[20] and Liu et al.[24] For example, in Ref. 41, Schlieren experiments were performed for a rotor and a second disturbance was seen

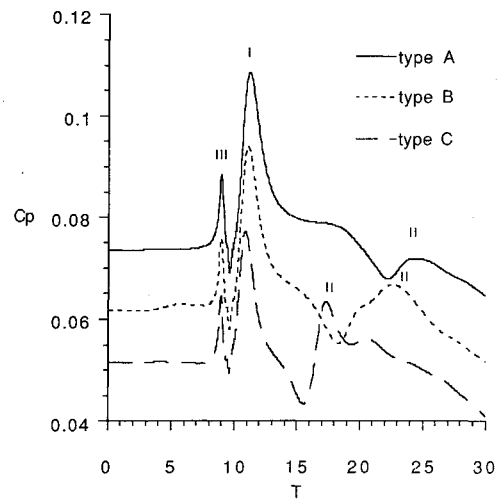

Fig. 8 Comparison of the near-field BVI noise for types A, B, and C [point P ($x = -0.3000$, $y = -0.17478$)].

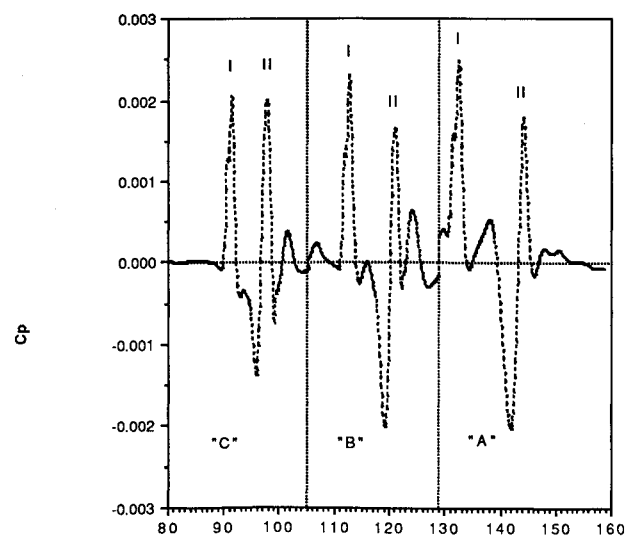

Fig. 9 Comparison of the near-field BVI noise for types A, B, and C [point O ($r = 20$ chords, $\theta = 30$ deg, span = 8 chords)].

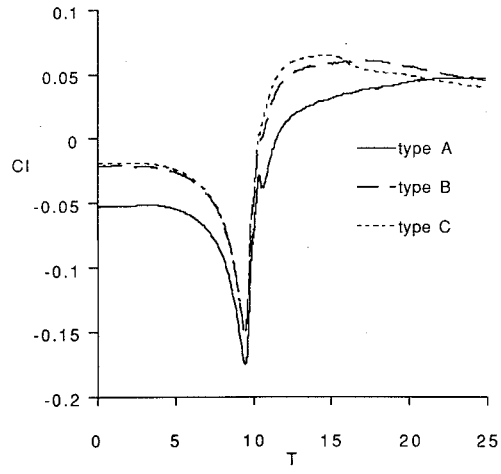

Fig. 10 Comparison of the $C_l(T)$ signal for BVI, types A, B, and C.

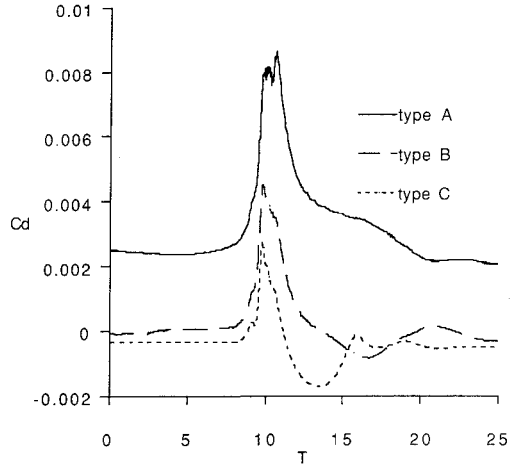

Fig. 11 Comparison of the $C_d(T)$ signal for BVI, types A, B, and C.

to propagate in the far field as postulated by computational results. Disturbance III is considered to be a standing disturbance due to the vortex passage and it is not a propagating wave. Thus, this disturbance disappears as we move from the midfield (Fig. 8) to the far field (Fig. 9).

From Figs. 8 and 9, we can see that disturbance I increases slightly with increasing Mach number. We should also bear in mind that the definition of C_p includes division by M^2, so the effect of the Mach number is stronger than it appears in the above figures. Disturbance II exists also for types A and B shock motions, because it is caused by the movement of the entire supersonic pocket and seems to be magnified as we move into the far field. It also appears to be decreasing as we move from type C to type A. However, if we measure it from peak to peak (instead of just reaching the maximum value), it still increases but at a lower rate than disturbance I. Disturbance III is almost the same for the three cases, which seems reasonable since the same vortex strength is used.

Figure 10 shows the lift coefficient $C_l(T)$ for types A, B, and C. We can see that their shapes relate well to the first disturbances shown in previous figures. Specifically, the total C_l change for the type A shock motion is much higher than that for type C. Thus, we can deduce that disturbance I is most probably related to C_l.

The drag coefficient C_d will be discussed next. It is well known that in uniform subcritical inviscid flow C_d is zero. It should be noted though that C_d is not zero for subcritical inviscid BVI due to the vortex acceleration. When the flow becomes supercritical, then the inviscid C_d is higher because of the formation of supersonic pockets. This was verified by running the code for subcritical and supercritical cases. C_d

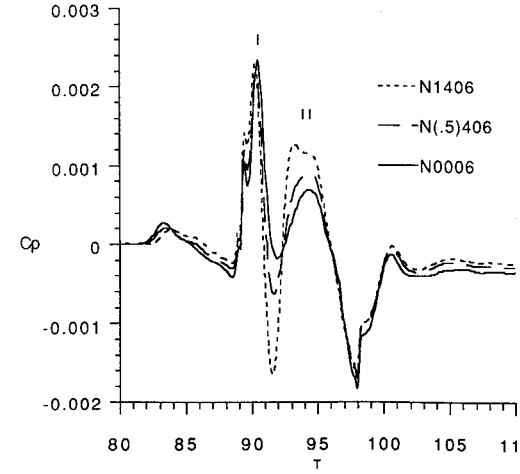

Fig. 12 Comparison of the far-field noise for NACA-0006 (α = 1.051 deg), NACA-(0.5)406 (α = 0.536 deg), and NACA-1406 (α = 0 deg), initial C_l = 0.229 in all cases [point O (r = 20 chords, θ = 30 deg, span = 8 chords)].

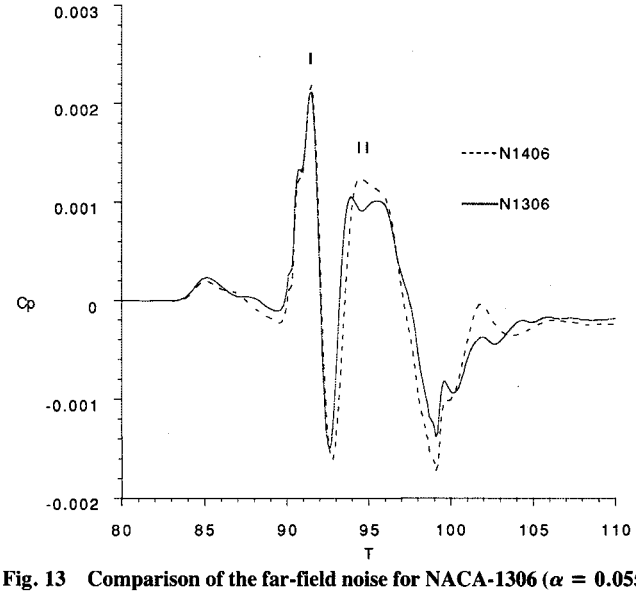

Fig. 13 Comparison of the far-field noise for NACA-1306 (α = 0.055 deg) and NACA-1406 (α = 0 deg), initial C_l = 0.229 in both cases [point O (r = 20 chords, θ = 30 deg, span = 8 chords)].

can be easily calculated in terms of the pressure distribution. Figure 11 shows $C_d(T)$ for types A, B, and C. The C_d signal seems to catch some part of the second disturbance, whereas C_l does not. The two disturbances were also detected by Liu et al.,[24] for some BVI cases using a thin-layer Navier-Stokes code, but no explanation was offered about their existence. These disturbances are easier to see in the case of an oscillating flap,[15] because there the periodicity of the motion is well defined. Thus, we can conclude that the second disturbance is most probably related to the fluctuating C_d caused mainly by the movement of the supersonic pocket.

In order to verify the above arguments, we compared results from airfoils with the same thickness distribution (i.e., same family) but different camber, in conditions producing the same lift (i.e., different angle of attack). Figure 12 compares the $C_p(T)$ BVI signals for the far field (point O) for a NACA-1406 airfoil at an angle of attack $\alpha = 0$ deg, for a NACA-(0.5)406 at $\alpha = 0.536$ deg, and for a NACA-0006 at $\alpha = 1.051$ deg. These conditions, with a standing vortex upstream, produce an initial $C_l = 0.229$. In fact, the entire unsteady lift $C_l(T)$ for these cases is almost the same, whereas the unsteady drag $C_d(T)$ is not. All of the airfoils have a type A shock motion for these conditions. We can see from Fig. 12 that disturbance I remains unchanged, whereas disturbance II does change,

becoming higher as the camber increases. This agrees with our earlier discussion of lift and drag forces.

We also investigated the effect of the point of maximum camber. In Fig. 13, we compared the $C_p(T)$ BVI signals for the far field (point O) for NACA airfoils with different point of maximum camber: NACA-1306 and NACA-1406, for angles of attack that produce the same lift: $\alpha = 0.055$ and 0 deg, respectively. We can see from Fig. 13 that disturbance I remains unchanged, whereas disturbance II becomes larger as the point of maximum camber moves downstream. Thus, the NACA-1406 airfoil has the larger disturbance II.

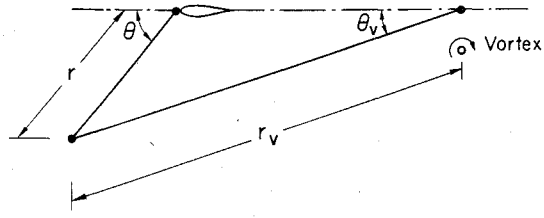

Fig. 14 Relation between an airfoil-fixed and vortex-fixed coordinate system.

From Figs. 12 and 13, we can conclude that disturbance I is related to the lift and disturbance II is related to the details of the airfoil shape, which produce a different supersonic pocket and thus a different drag. Symmetric airfoils and airfoils with the point of maximum camber further upstream give a lower value of disturbance II, for the same lift.

A parametric study showed[26] that the vortex strength has a strong effect on the noise signal, whereas the vortex miss distance has only a weak effect. The maximum airfoil thickness and the details of airfoil shape were also found to be important. A more detailed parametric study is currently being carried out.

The directivity of the noise signal in the far field is very complicated, as has been shown by experimental studies. Most of these experiments are also three dimensional, which makes it very difficult to compare. For example, in Ref. 42, it was shown for a model helicopter rotor that the maximum signal can have a different direction if the advance ratio μ is varied.

Directivity is studied in a vortex-fixed coordinate system keeping the distance from the vortex r_v constant (r_v = 50 chords). The relationship between the angles θ and θ_v in an airfoil-fixed and a vortex-fixed coordinate system is shown in Fig. 14. The $C_p(t)$ signal for different directions is plotted in

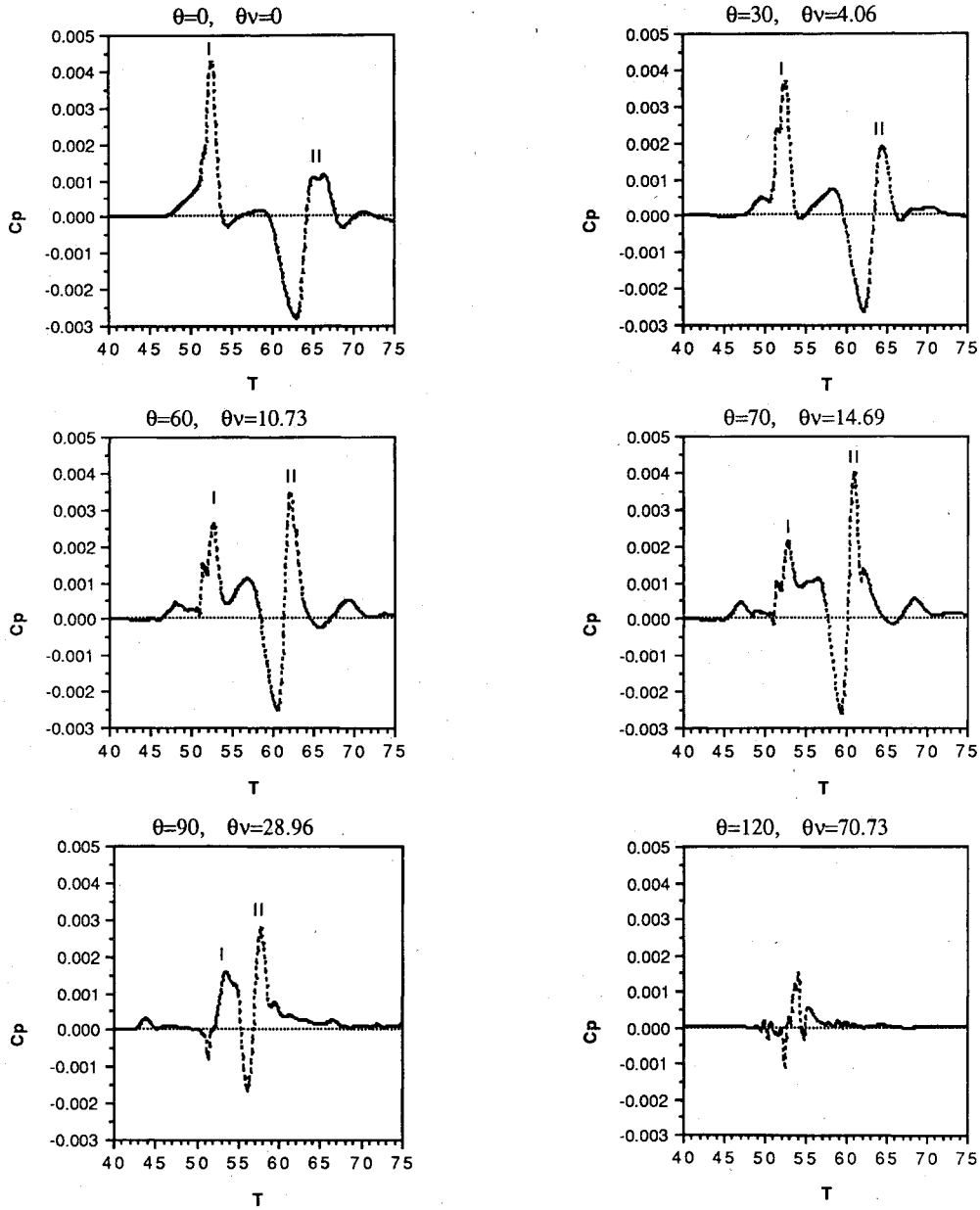

Fig. 15 BVI noise directivity for type A (r_v = 50 chords, span = 4 chords).

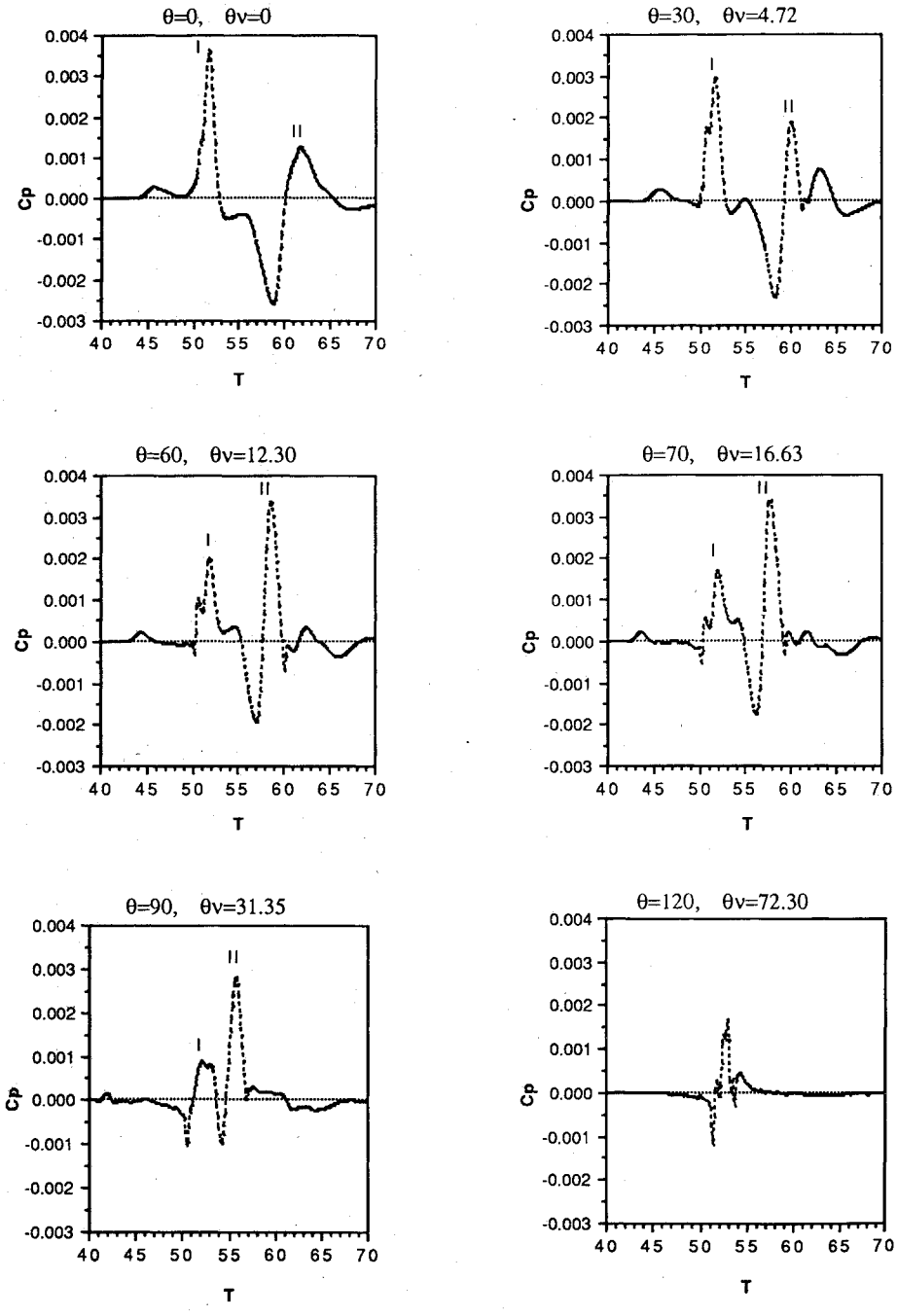

Fig. 16 BVI noise directivity for type B (r_v = 50 chords, span = 4 chords).

Figs. 15–17 for types A, B, and C shock motion, respectively (note that span = 4 chords for this case). By inspecting the plots, we can see that disturbance I is getting weaker as the direction angle θ increases from 0 to 90 deg (forward directivity). Disturbance II is getting stronger as the direction angle θ increases from 0 to 90 deg (downward directivity). The two disturbances also move closer as the angle θ is increased, and finally almost merge at θ = 120 deg. This implies a different origin. If the origin of disturbance I is at the airfoil leading edge, the origin of disturbance II is probably somewhere downstream since this disturbance is related to the movement of the supersonic pocket.

It should be noted that for an oscillating flap[15] the opposite directivity was observed: downward for disturbance I and forward for disturbance II. Thus, it was concluded that disturbance I is due to the dipole produced from oscillating lift and disturbance II is produced from oscillating drag. If we run a subcritical case, then disturbance II disappears, as expected, and the directivity of disturbance I is downward (disturbance increases as θ is increased from 0 to 90 deg). In both disturbances, the directivity observed was not expected to be exactly the one described by a pure dipole, because of various nonlinearities (i.e., supersonic pocket) and source noncompactness. However, a main dipole-like behavior, as the one detected in the oscillating flap case,[15] was expected. The reason that the directivity is different for an oscillating flap and BVI seems to be related to the difference in phase between the two disturbances. Disturbance II has a higher frequency than disturbance I and also a different phase with respect to disturbance I. Thus, it may add or subtract differently in different directions for various cases (i.e., diffraction). In the oscillating-flap case, the frequency and the phase difference are forced better than they are in the BVI case.

Consider next the noise signals resulting from types A, B, and C shock motion (Figs. 15–17, respectively). The two disturbances keep approaching each other as angle θ is in-

creased because of the different disturbance origin. Angles $\theta = 70$ deg and 60 deg seem to give the maximum signal, if we measure from peak to peak, for types A and B, respectively. (If we only look at the maximum absolute value, then $\theta = 0$ deg seems to produce the greatest noise.) For the case of type C, we can see that the entire region between $\theta = 60$ deg and $\theta = 90$ deg produces about the same noise. For subsonic cases (not shown), the maximum noise is 90 deg, as it was mentioned above.

Figure 18 shows the directivity of the BVI for a NACA-0006 airfoil. In this case, the two disturbances are closer to each other than the previous NACA-64A006 cases. If we increase θ, the two disturbances now fall on top of each other more quickly ($\theta = 90$ deg). The noise becomes maximum at $\theta = 90$ deg, but still the noise at $\theta = 60$ deg and 70 deg is not much lower. Similar observations can be made for all of the other four-digit airfoils tried [e.g., 1306, 1406, (0.5)406].

From the preceding discussion of BVI noise directivity, we can conclude that the maximum noise occurs at around $\theta =$ 60–90 deg ($\theta_v = 10$–30 deg), and depends on both disturbances I and II, but also on the phase difference between the two disturbances, which can be different for various airfoil shapes.

To isolate the effect of disturbance II in the maximum noise, we compared (Fig. 19) the $C_p(T)$ signal at the same point ($\theta = 90$ deg and $r_v = 50$ chords) for NACA airfoils 0006, (0.5)406, and 1406 for the conditions specified before for Fig. 12 (i.e., same lift). It can be noted that the two disturbances are almost merged at this point. We can also see that the NACA-1406 airfoil has a larger signal, which is consistent with the fact that the same airfoil has a larger disturbance II as shown in Fig. 12.

In Fig. 20, we compared the signal for NACA airfoils with different points of maximum camber: NACA-1306 and NACA-1406, for angles of attack that produce the same lift: $\alpha = 0.055$ and 0 deg, respectively. We looked at the point of maximum noise: $\theta = 90$ deg and $r_v = 50$ chords. We can see that the NACA-1406 airfoil has the larger signal, as expected since

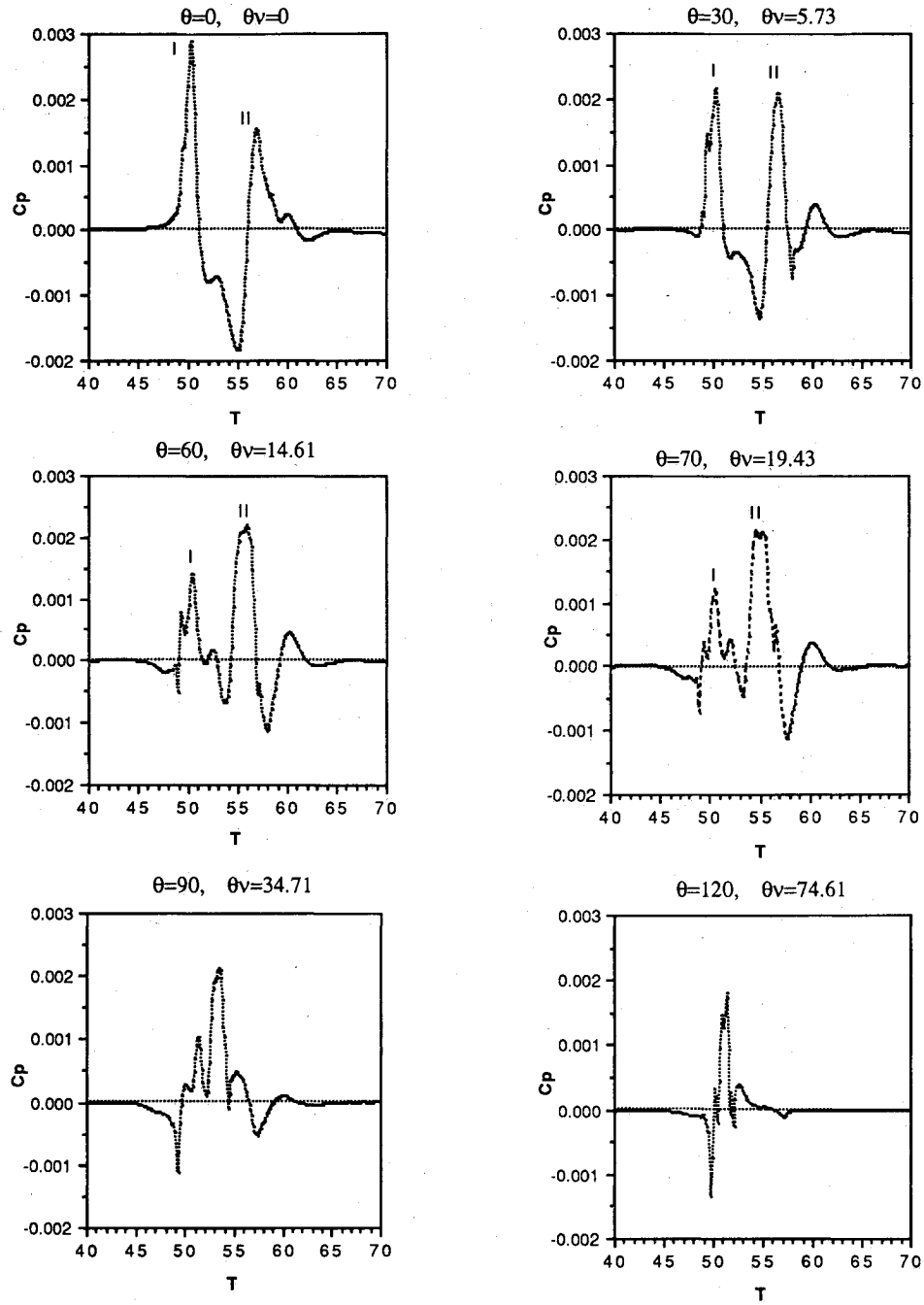

Fig. 17 BVI noise directivity for type C ($r_v = 50$ chords, span = 4 chords).

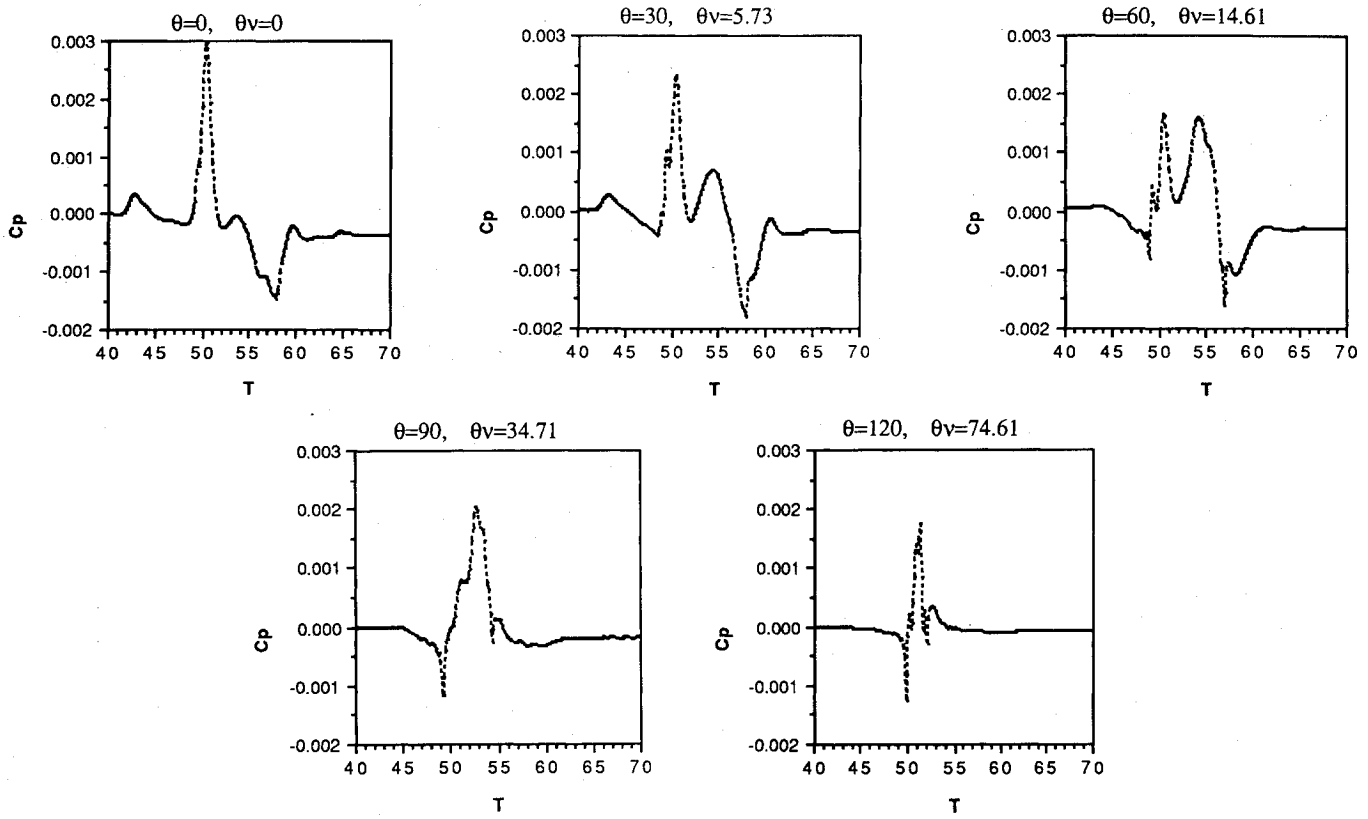

Fig. 18 BVI noise directivity for NACA-0006 (r_v = 50 chords, span = 4 chords).

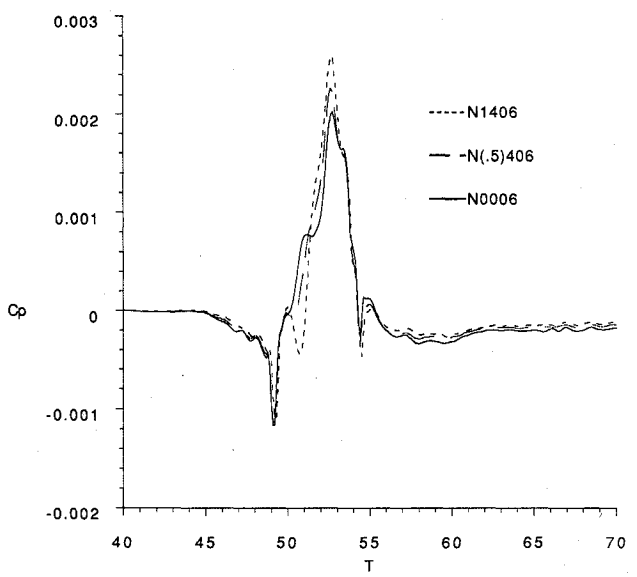

Fig. 19 Comparison of the far-field noise for NACA-0006 (α = 1.051 deg), NACA-(0.5)406 (α = 0.536 deg), and NACA-1406 (α = 0 deg), initial C_l = 0.220 in all cases (θ = 90 deg, r_v = 50 chords, span = 4 chords).

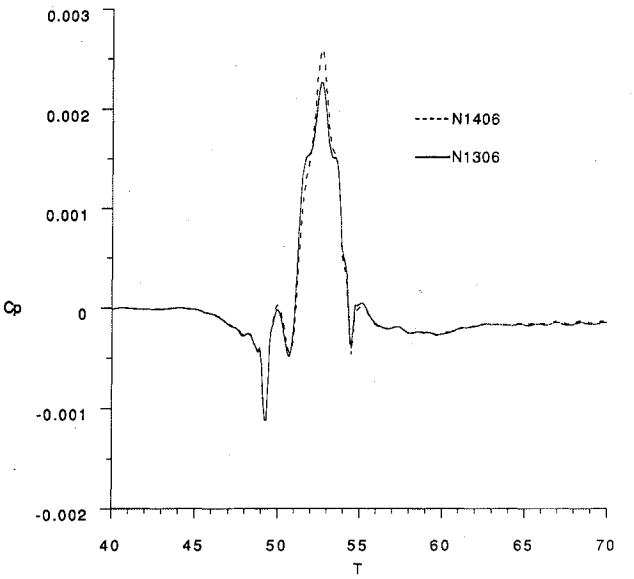

Fig. 20 Comparison of the far-field noise for NACA-1306 (α = 0.055 deg) and NACA-1406 (α = 0 deg), initial C_l = 0.229 in both cases (θ = 90 deg, r_v = 50 chords, span = 4 chords).

the same airfoil has a larger disturbance II as shown in Fig. 13.

We also ran the previously used four-digit airfoils at subsonic Mach numbers at conditions producing the same lift. They all produced the same BVI disturbance at all angles, as expected (no disturbance II was observed). In conclusion, symmetric airfoils and airfoils with a point of maximum camber farther upstream seem to give less BVI noise for transonic conditions producing the same lift.

A direct comparison of the results obtained from the different methods (from small disturbance to Navier-Stokes equations) shows that the results are very similar.[7] In fact, the further away we move from the airfoil surface the results tend to coincide. Thus, we expect that our conclusions will also hold if more accurate Euler/Navier-Stokes predictions are used. Three-dimensionality will, of course, influence the results. Some of the presented comparisons are expected to hold for three-dimensional cases, but only actual three-dimensional calculations (e.g., Ref. 43) can show that.

Conclusions

An existing numerical finite-difference code VTRAN2 was modified to analyze noise due to transonic BVI. The two-dimensional unsteady transonic small-disturbance equation

was solved numerically using ADI techniques with monotone switches, including viscous effects due to shock-boundary interaction and the cloud-in-cell method for the simulation of the vortex. The Kirchhoff's method was used to extend the numerically calculated two-dimensional near-field aerodynamic results to the three-dimensional linear acoustic far field.

The viscous effect (shock/boundary-layer interaction) on BVI noise was studied and was found to have only a weak influence. The effect of the three types of unsteady shock motion (A, B, and C) was also investigated. The unsteady pressure coefficients $C_p(t)$ showed the existence of two main disturbances. The first one (I) is believed to be associated with the fluctuating lift coefficient C_l and has a strong forward directivity, while the second (II) is believed to be associated with the fluctuating drag coefficient C_d caused by the movement of the supersonic pocket and has a strong downward directivity. The maximum radiation occurs at an angle θ between 60 and 90 deg below the horizontal for an airfoil-fixed coordinate system, and depends on both disturbances I and II and the details of the airfoil shape. Symmetric airfoils, and airfoils with a point of maximum camber further upstream, seem to give less BVI noise for conditions producing the same lift.

It is hoped that this work can contribute toward the better understanding of the mechanisms of noise due to transonic BVI. In the future, we plan to study the influence of the details of airfoil shape, especially near the leading edge. We will also include the effects of an oscillating airfoil at the same time with a BVI that can be useful in actual helicopter cases (feathering).

Acknowledgments

The authors want to thank P. M. Goorjian from NASA Ames Research Center for providing the new version of LTRAN2. The calculations were performed at the computational facilities of Minnesota Supercomputer Institute (MSI) and at the Cornell University Production Supercomputer Facility of the Center for Theory and Simulation in Science and Engineering. Finally, this research was supported by a Grant-in-Aid of Research from the Graduate School of the University of Minnesota, and NASA Grants NAG 2-588 and NAG 2-646. C. Kitaplioglu was the technical monitor and his suggestions during the course of the research are greatly appreciated by the authors.

References

[1]George, A. R., "Helicopter Noise: State-of-the-Art," *Journal of Aircraft*, Vol. 15, No. 11, 1978, pp. 707–715.

[2]Schlinker, R. H., and Amiet, R. K., "Rotor-Vortex Interaction Noise," NASA CR-3744, Oct. 1983.

[3]Schmitz, F. H., and Yu, Y. H., "Helicopter Impulsive Noise: Theoretical and Experimental Status," *Recent Advances in Aeroacoustics*, edited by A. Krothapalli and C. A. Smith, Springer-Verlag, New York, 1986, pp. 149–243.

[4]George, A. R., Smith, C. A., Maisel, M. D., and Brieger, J. T., "Tilt Rotor Aircraft Aeroacoustics," *Proceedings of the 45th Annual Forum of the American Helicopter Society*, American Helicopter Society, Alexandria, VA, 1989.

[5]Poling, D. R., Dadone, L., and Telionis, D. P., "Blade-Vortex Interaction," *AIAA Journal*, Vol. 27, No. 6, 1989, pp. 694–699.

[6]George, A. R., and Chang, S. B., "Noise Due to Transonic Blade-Vortex Interactions," *Proceedings of the 39th Annual National Forum of the American Helicopter Society*, Paper A-83-39-50-D000, 1983.

[7]George, A. R., and Chang, S. B., "Flowfield and Acoustics of Two-dimensional Transonic Blade-Vortex Interactions," AIAA Paper 84-2309, Oct. 1984.

[8]Ballhaus, W. F., and Goorjian, P. M., "Implicit Finite-Difference Computations of Unsteady Transonic Flows about Airfoil," *AIAA Journal*, Vol. 15, No. 12, 1977, pp. 1728–1735.

[9]Rizzetta, D. P., and Chin, W. C., "Effect of Frequency in Unsteady Transonic Flow," *AIAA Journal*, Vol. 17, No. 7, 1979, pp. 779–781.

[10]Guruswamy, P., and Goorjian, P. M., "Effects of Viscosity on Transonic Aerodynamic and Aeroelastic Characteristics of Oscillating Airfoils," *AIAA Journal*, Vol. 21, No. 9, 1984, pp. 700–707.

[11]Goorjian, P. M., Meagher, M. E., and Van Buskirk, R. D., "Monotone Switches in Implicit Algorithms for Potential Equations Applied to Transonic Flows," *AIAA Journal*, Vol. 23, No. 4, 1985, pp. 492–498.

[12]Goorjian, P. M., and Van Buskirk, R. D., "Second-Order-Accurate Spatial Differencing for the Transonic Small-Disturbance Equation," *AIAA Journal*, Vol. 23, No. 11, 1985, pp. 1693–1699.

[13]Lyrintzis, A. S., and George, A. R., "VTRAN2: Computation of Two-dimensional Blade-Vortex Interactions Using the Unsteady Small-Disturbance Equation (User's Manual)," Cornell Univ., Ithaca, NY, March 1986.

[14]Lyrintzis, A. S., "Transonic Blade-Vortex Interactions," Ph.D. Dissertation, Mechanical and Aerospace Engineering Dept., Cornell Univ., Ithaca, NY, Jan. 1988.

[15]Lyrintzis, A. S., and Xue, Y., "Acoustics of Transonic Flow Around an Oscillating Flap," *Journal of Fluids Engineering* (submitted for publication).

[16]McCroskey, W. J., and Goorjian, P. M., "Interactions of Airfoils with Gusts and Concentrated Vortices in Unsteady Transonic Flow," AIAA Paper 83-1691, July 1983.

[17]Srinivasan, G. R., McCroskey, W. J., and Kutler, P., "Numerical Simulation of the Interaction of a Vortex with Stationary Airfoil in Transonic Flow," AIAA Paper 84-0254, Jan. 1984.

[18]Sankar, N. L., and Tang, W., "Numerical Solution of Unsteady Viscous Flow Past Rotor Sections," AIAA Paper 85-129, Jan. 1985.

[19]Srinivasan, G. R., McCroskey, W. J., and Baeder, J. D., "Aerodynamics of Two-Dimensional Blade-Vortex Interaction," *AIAA Journal*, Vol. 24, No. 10, 1986, pp. 1569–1576.

[20]Owen, S. T., and Shenoy, R. K., "Numerical Investigation of Two-Dimensional Blade-Vortex Interaction," *Proceedings of the AHS National Specialist's Meeting on Aerodynamics and Aeroacoustics*, American Helicopter Society, Alexandria, VA, 1987.

[21]Damodaran, M., and Caughey, D. A., "A Finite-Volume Euler Calculation of the Aerodynamics of Transonic Airfoil-Vortex Interaction," *AIAA Journal*, Vol. 26, No. 11, 1988, pp. 1346–1353.

[22]Baeder, J. D., McCroskey, W. J., and Srinivasan, G. R., "Acoustic Propagation Using Computational Fluid Dynamics," *Proceedings of the 42nd Annual Forum of the American Helicopter Society*, American Helicopter Society, Alexandria, VA, Vol. 1, 1986, pp. 551–562.

[23]Baeder, J. D., "Computation of Nonlinear Acoustics in Two-Dimensional Blade-Vortex Interactions," *Proceedings of the 13th European Rotorcraft Forum*, Association Aeronautique et Astronautique de France, 1987, pp. 1-1-1–1-1-6.

[24]Liu, N. S., Davoudzadeh, F., Briley, W. R., and Shamroth, S. J., "Navier-Stokes Simulation of Transonic Blade-Vortex Interactions," *Proceedings of the International Symposium on Nonsteady Fluid Dynamics (ASME)*, edited by J. A. Miller and D. P. Telionis, American Society of Mechanical Engineers, New York, 1990, pp. 177–186.

[25]George, A. R., and Lyrintzis, A. S., "Acoustics of Transonic Blade-Vortex Interactions," *AIAA Journal*, Vol. 26, No. 7, 1988, pp. 769–776.

[26]Lyrintzis, A. S., and George, A. R., "Far-Field Noise of Transonic Blade-Vortex Interactions," *American Helicopter Society Journal*, Vol. 34, No. 3, 1989, pp. 30–39.

[27]Lyrintzis, A. S., and George, A. R., "The Use of Kirchhoff Method in Acoustics," *AIAA Journal*, Vol. 27, No. 10, 1989, pp. 1451–1453.

[28]Lyrintzis, A. S., and George, A. R., "Study of Transonic Blade-Vortex Interaction Noise," *Noise Control Engineering Journal*, Vol. 32, No. 3, 1989, pp. 105–109.

[29]Lyrintzis, A. S., and Xue, Y., "Noise Mechanisms of Transonic Blade-Vortex Interactions," *Proceedings of the American Helicopter Society 46th Annual Forum*, American Helicopter Society, Alexandria, VA, 1990.

[30]Ballhaus, W. F., "Some Recent Progress in Transonic Flow Computations," *Numerical Methods in Fluid Dynamics*, edited by H. J. Wirz, and J. J. Smolderen, McGraw Hill, New York, 1978, pp. 155–235.

[31]Poling, D. R., and Telionis, D. P., "The Response of Airfoils to Periodic Disturbances—The Unsteady Kutta Condition," *AIAA Journal*, Vol. 24, No. 2, 1986, pp. 193–199.

[32]Chang, S. B., "Aerodynamics and Acoustics of Transonic Two-Dimensional Blade-Vortex Interactions," Ph.D. Dissertation, Mechanical and Aerospace Engineering Dept., Cornell Univ., Ithaca, NY, Jan. 1985.

[33]Rizzetta, D. P., "Procedures for the Computation of Unsteady

Transonic Flow Including Viscous Effects," NASA CR-166249, Jan. 1982.

[34]Morgans, R. P., "The Kirchhoff Formula Extended to a Moving Surface," *Philosophical Magazine*, Vol. 9 (s.7, No. 55), 1930, pp. 141–161.

[35]Morino, L., "A General Theory of Unsteady Compressible Potential Aerodynamics," NASA CR-2464, Dec. 1974.

[36]Morino, L., "Steady Oscillatory, and Unsteady Subsonic and Supersonic Aerodynamics—Production Version 1.1 (SOUSSA-P, 1.1), Vol. 1, Theoretical Manual," NASA CR-159130, Jan. 1980.

[37]Farassat, F., and Myers, M. K., "Extension of Kirchhoff's Formula to Radiation from Moving Surfaces," *Journal of Sound and Vibration*, Vol. 123, No. 3, 1988, pp. 451–460.

[38]Tijdeman, H., "Investigations of the Transonic Flow Around Oscillating Airfoils," National Aerospace Laboratory, NLR TR 77090-U, The Netherlands, 1977.

[39]Tangler, J. L., "Schlieren and Noise Studies of Rotors in Forward Flight," The 33rd Annual National Forum of the American Helicopter Society, Paper 77. 33-05, Washington, DC, May 1977.

[40]Caradonna, F. X., Laub, G. H., and Tung, C., "An Experimental Investigation of the Parallel Blade-Vortex Interaction," 10th European Rotorcraft Forum, The Hague, The Netherlands, Aug. 1984.

[41]Shenoy, R. K., "Aeroacoustic Flowfield and Acoustics of a Model Helicopter Tail Rotor at a High Advance Ratio," *Proceedings of the 45th Annual Forum of the American Helicopter Society*, American Helicopter Society, Alexandria, VA, 1989.

[42]Martin, M. R., and Splettstoesser, W. R., "Acoustic Results of the Blade-Vortex Interaction Acoustic Test of a 40-Percent Model Rotor in the DMW," *Proceedings of the American Helicopter Society National Specialists' Meeting on Aerodynamics and Aeroacoustics*, American Helicopter Society, Alexandria, VA, 1987.

[43]Tadghighi, H., Hassan, A. A., and Charles, B., "Prediction of Blade-Vortex Interaction Noise Using Airloads Generated by a Finite-Difference Technique," *Proceedings of the 46th Annual Forum of the American Helicopter Society*, American Helicopter Society, Alexandria, VA, Vol. I, 1990, pp. 367–378.